Divergence Free High Order Filter Methods for the Compressible MHD Equations*

H. C. Yee[1] and Björn Sjögreen[2]

[1] NASA Ames Research Center, USA *yee@nas.nasa.gov*
[2] Royal Institute of Technology, Sweden *bjorns@nada.kth.se*

Abstract: The generalization of a class of low-dissipative high order filter finite difference methods for long time wave propagation of shock/turbulence/combustion compressible viscous gas dynamic flows to compressible MHD equations for structured curvilinear grids has been achieved. The new scheme is shown to provide a natural and efficient way for the minimization of the divergence of the magnetic field numerical error. Standard divergence cleaning is not required by the present filter approach. For certain MHD test cases, divergence free preservation of the magnetic fields has been achieved.

1 Introduction

An integrated approach for the control of numerical dissipation in high order finite difference schemes in structured curvilinear grids for the compressible Euler and Navier-Stokes equations has been developed and verified by the authors and collaborators [27, 28, 18, 29, 21]. These schemes are suitable for complex multiscale compressible viscous flows, especially for high speed turbulence combustion and acoustics problems. Standard high-resolution shock-capturing schemes are too dissipative for these types of flow problems. For the performance of these schemes on the aforementioned flows, see [27, 28, 18, 29, 21, 19, 20] and references cited therein. Basically, the scheme consists of sixth-order or higher non-dissipative spatial difference operators as the base scheme. To control the amount and types of numerical dissipation, an artificial compression method (ACM) indicator or multiresolution wavelets are used as sensors to adaptively limit the amount and to aid in the selection and/or blending of the appropriate types of numerical dissipation to be used. This adaptive control of numerical dissipation is accomplished by a filter step after the completion of each full time step integration of the base scheme. Hereafter, we refer to these schemes as the high order ACM-filter and WAV-filter methods.

The type of base schemes used in the high order ACM-filter and WAV-filter methods is divergence free preserving for the magnetohydrodynamics (MHD) equations. However, straightforward application of the filter step to the MHD equations will not automatically preserve the divergence free magnetic field condition. With careful modification of the gas dynamic scheme, the filter mechanism offers several natural and efficient alternatives (without the standard divergence cleaning procedures) for minimizing the $\nabla \cdot \mathbf{B}$ numerical error which are not easily attainable without additional work in the standard high-resolution shock-capturing schemes. The focus of this paper is to present a filter approach that exhibits divergence free preservation for certain test cases. Extensive grid convergence comparisons with standard high-resolution shock-capturing schemes will be shown.

* Proceedings of the International Conference on High Performance Scientific Computing, March 10-14, 2003, Hanoi, Vietnam. Part of this work was performed while the second author was a RIACS visiting scientist at NASA Ames Research Center.

2 Relevance

This paper is concerned with the compressible MHD equations, henceforth, for ease of reference, referred to simply as MHD equations. Throughout the paper, the term "$\nabla\cdot\mathbf{B}$ numerical error" refers to the "amount of non-zero value of the discretized form of $\nabla\cdot\mathbf{B}$ of the underlying scheme". The following discussion pertains to schemes involving the use of Riemann solvers or the eigen-structure of the MHD equations. In addition, our discussion is restricted to the finite difference formulation for structured grids.

An important ingredient in our method is the use of the dissipative portion of high-resolution shock-capturing schemes as part of the nonlinear filters. These nonlinear filters involve the use of approximate Riemann solvers. We will therefore first present a new form of high-resolution shock-capturing schemes for the conservative MHD equations using the non-conservative eigensystem.

Consider the 3-D conservative and non-conservative forms of the ideal compressible MHD equations in Cartesian grids,

$$\begin{pmatrix} \rho \\ \rho u \\ \rho v \\ \rho w \\ e \\ B_x \\ B_y \\ B_z \end{pmatrix}_t + \text{div} \begin{pmatrix} \rho\mathbf{u} \\ \rho\mathbf{u}\mathbf{u}^T + (p + B^2/2)I - \mathbf{B}\mathbf{B}^T \\ \mathbf{u}(e + p + B^2/2) - \mathbf{B}(\mathbf{u}^T\mathbf{B}) \\ \mathbf{u}\mathbf{B}^T - \mathbf{B}\mathbf{u}^T \end{pmatrix} = 0 \quad \text{(conservative)}, \tag{1}$$

and

$$\begin{pmatrix} \rho \\ \rho u \\ \rho v \\ \rho w \\ e \\ B_x \\ B_y \\ B_z \end{pmatrix}_t + \text{div} \begin{pmatrix} \rho\mathbf{u} \\ \rho\mathbf{u}\mathbf{u}^T + (p + B^2/2)I - \mathbf{B}\mathbf{B}^T \\ \mathbf{u}(e + p + B^2/2) - \mathbf{B}(\mathbf{u}^T\mathbf{B}) \\ \mathbf{u}\mathbf{B}^T - \mathbf{B}\mathbf{u}^T \end{pmatrix} = -(\nabla\cdot\mathbf{B}) \begin{pmatrix} 0 \\ B_x \\ B_y \\ B_z \\ \mathbf{u}^T\mathbf{B} \\ u \\ v \\ w \end{pmatrix} \quad \text{(non-conservative)}, \tag{2}$$

where the velocity vector $\mathbf{u} = (u, v, w)^T$, the magnetic field vector $\mathbf{B} = (B_x, B_y, B_z)^T$, ρ is the density, and e is the total energy. The notation $B^2 = B_x^2 + B_y^2 + B_z^2$ is used. The pressure is related to the other variables by

$$p = (\gamma - 1)(e - \frac{1}{2}\rho(u^2 + v^2 + w^2) - \frac{1}{2}(B_x^2 + B_y^2 + B_z^2)).$$

For plasmas, γ is usually equal to 5/3 (for monatomic gases). The vector on the right hand side of (2) is the non-conservative portion of the MHD equations [16, 17, 24]. The non-conservative term is proportional to $(\nabla\cdot\mathbf{B})$. Physically, it is zero if $\nabla\cdot\mathbf{B} = 0$ initially. In symbolic form, the conservative and non-conservative forms can be written as

$$U_t + \nabla\cdot\mathbf{F} = 0,$$

$$U_t + \nabla\cdot\mathbf{F} = S,$$

where U is the corresponding state vector, $\mathbf{F}$ is the conservative inviscid flux vector tensor and S is the non-conservative portion of the equations in (2). The non-conservative term S can also be written as $S = \sum_{i=1}^{3} N_i(U)U_{x_i}$, where the notation $(x_1, x_2, x_3) = (x, y, z)$ is used. The curvilinear grid formulation follows the same methodology as in [25].

2.1 Divergence Condition

The $\nabla \cdot \mathbf{B} = 0$ condition is an initial constraint for the MHD equations, and it is **not** part of the MHD differential system. This is unlike the divergence-free condition of the velocities for the incompressible Euler or Navier-Stokes equations which is part of the differential system and is needed to close the system and must be explicitly enforced. For the MHD equations with $\nabla \cdot \mathbf{B} = 0$ as the initial data, all one needs is to construct schemes with the discretized form of $\nabla \cdot \mathbf{B}$ on the order of the truncation error, which goes to zero when the grid is refined. Unfortunately, straightforward extension of existing gas dynamic schemes to the MHD equations does not necessarily preserve the divergence-free condition.

Presently, there are basically two camps in solving the multi-dimensional MHD equations; namely, that which solves the conservative form, and the one which solves the non-conservative symmetrizable form [10, 16, 17]. For both forms of the MHD equations, high-resolution shock-capturing methods suffer from the need to perform extra work to drive the $\nabla \cdot \mathbf{B}$ numerical error down to machine zero. The popular approaches for minimizing the $\nabla \cdot \mathbf{B}$ numerical error include augmenting an extra PDE to the system [2], using variants of the staggered approach of K.S. Yee [31, 6, 7, 4] and using a projection method [32]. There is a key advantage to solving the conservative equations over the non-conservative equations, since the conservative form guarantees correct propagation speeds and locations of discontinuities. The disadvantage is that the conservative form is a non-strictly hyperbolic system with non-convex inviscid fluxes. There exist states (e.g., triple umbilic points for 1-D) for which the Jacobian of the flux of the conservative form does not have a complete set of eigenvectors. In this paper and companion papers [22, 30], both the non-conservative and conservative forms of the multidimensional compressible MHD system are considered.

2.2 Conservative and Non-Conservative Formulations Involving the Use of Approximate Riemann Solvers

For convenience of presentation we will describe our numerical methods for the x-flux on a uniform grid. A more detailed discussion can be found in [22]. Let $A(U)$ denote the Jacobian $\partial F/\partial U$ with the understanding that the present F and S are the x-component of the 3-D description above. For later discussion we write the non-conservative S term in the x-direction as $N(U)U_x$.

Gallice [9] and Cargo and Gallice [1] observed that seven of the eigenvalues and eigenvectors are identical for the "conservative" Jacobian matrix A and the "non-conservative" Jacobian matrix $(A-N)$. The eighth eigenvector of A of the conservative system (which is distinct from the non-conservative system) associated with the degenerate zero eigenvalue can sometimes coincide with one of the other eigenvectors, thereby, making it impossible to define the MHD Roe's approximate Riemann solver in the standard way. The eigenvectors of the non-conservative Jacobian $(A-N)$ always form a complete basis, and can be obtained from analytical formulas [9, 1]. A Roe type average state was developed in [9, 1].

We formulate our scheme together with the Gallice form of the MHD Roe's approximate Riemann solver in curvilinear grids for both the conservative and non-conservative MHD equations. We propose to use the non-conservative form of the eigen-decomposition but with the degenerate eigenvalue replaced by an entropy correction [11, 26] of what was supposed to be the zero eigenvalue for the conservative form (e.g., a small parameter ϵ that is scaled by the largest eigenvalue of $A(U)$). Our rationale for doing this is that only the eighth eigenvector of the non-conservative form is not the same as the eighth

eigenvector for the conservative form. The incorrect eigenvector for the conservative form will be multiplied by an eigenvalue which is close to zero (the eigenvalue will not be exactly zero when an entropy correction is used). Thus the effect of a "false" eigenvector will be small. By using the eighth eigenvector of the non-conservative system instead, the difficulty of dealing with an incomplete set of eigenvectors for the conservative system can be avoided.

The conservative filter approach, and the conservative Harten-Yee, MUSCL and the fifth-order WENO [12] schemes used in this paper are formed by using the non-conservative eigen-decomposition described above in solving the conservative MHD equation set (1). The non-conservative filter approach, and the non-conservative Harten-Yee, MUSCL and WENO schemes are just the non-conservative eigen-decomposition in solving the non-conservative MHD equation set (2).

3 Description of High Order Filter Methods

Our high order ACM-filter and WAV-filter methods consist of two stages, a divergence-preserving base scheme stage (not involve the use of approximate Riemann solvers) and a filter stage (involve the use of approximate Riemann solvers). The filter stage can be divergence-free preserving depending on the type of filter operator being used and the method of applying the filter step. In order to have a good shock-capturing capability and improved nonlinear stability related to spurious high frequency oscillations, the blending of a high order nonlinear filter and a high order linear filter were proposed in our gas dynamic schemes. The nonlinear filter consists of the product of an ACM or wavelet sensor and the nonlinear dissipative portion of a high-resolution shock-capturing scheme. The high order linear filter is just the centered linear dissipative operator that is compatible with the order of the base scheme being used.

3.1 Divergence-Free Preserving Base Scheme Step

The first stage of the numerical method consists of a time step by a non-dissipative high order spatial and high order temporal base scheme operator L (e.g., a divergence-free preserving sixth-order central in space and fourth-order Runge-Kutta in time),

$$U^* = L(U^n), \tag{3}$$

where U^n is the numerical solution vector at time level n. When necessary, a high order linear numerical dissipation operator can be used. For example, a divergence-free preserving eighth-order linear dissipation with the sixth-order centered base scheme to approximate $F(U)_x$ is written as

$$\frac{\partial F}{\partial x} \approx D_{06}F_j + d\Delta x^7 (D_+D_-)^4 U_j, \tag{4}$$

where D_{06} is the standard sixth-order accurate centered difference operator, and D_+D_- is the standard second-order accurate centered approximation of the second derivative. The small parameter d is a scaled value in the range of 0.00001 to 0.01, depending on the flow problem, and has the sign which gives dissipation in the forward time direction. The operators are modified at boundaries in a stable way [29].

This highly accurate base scheme is employed to numerically preserve the divergence-free condition of the magnetic field (to the level of round-off error) for curvilinear grids. When the solution is smooth, the filter step might not be needed. Thus the use of a high order centered difference operator as the base scheme will perfectly preserve the

divergence-free condition. In this case the result will be the same, whether we solve the conservative system (1) or non-conservative system (2). Under a shock/shear and turbulence/combustion environment, the use of a dissipative portion of the shock-capturing scheme as part of the filter is necessary. In this case, a possible source of violation of the divergence-free condition can be from the filter step.

3.2 Adaptive Numerical Dissipation Filter Step

After the completion of a full time step of the divergence-free preserving base scheme stage, the second stage is to adaptively filter the solution by the **product** of "an ACM indicator or wavelet sensor" and the "**nonlinear dissipative portion** of a high-resolution shock-capturing scheme". The final update step after the filter can be written as (assume 1-D for ease of illustration)

$$U_j^{n+1} = U_j^* - \frac{\Delta t}{\Delta x}[H^f_{j+1/2} - H^f_{j-1/2}]. \tag{5}$$

The filter numerical flux vector is

$$H^f_{j+1/2} = R_{j+1/2}\overline{H}_{j+1/2}.$$

Here $R_{j+1/2}$ is the matrix of right eigenvectors of the Jacobian of the non-conservative MHD flux vector $(A_{j+1/2} - N_{j+1/2})$ evaluated at the Gallice average state $U^*_{j+1/2}$ as discussed in the previous subsection. The $\overline{H}_{j+1/2}$ are also evaluated from the same characteristic quantities derived from these eigenvectors using the Gallice average state based on the U^* values of (4). Due to the fact that the base scheme step is divergence free preserving and does not involve the use of approximate Riemann solvers, there is no difference in solving the conservative or non-conservative system for the filter approach. To reduce un-necessary computations (the non-conservative portion), the non-conservative filter approach only solves the conservative system on the base scheme step. Thus, the conservative and non-conservative filter approaches differ merely by the eighth eigenvalue.

Denote the elements of the vector $\overline{H}_{j+1/2}$ by $\overline{h}^l_{j+1/2}, l = 1, 2, ..., 8$. They have the form

$$\overline{h}^l_{j+1/2} = (\omega)^l_{j+1/2}(\phi^l_{j+1/2}). \tag{6}$$

Here $(\omega)^l_{j+1/2}$ is a sensor to activate the shock-capturing nonlinear filter. For example, $(\omega)^l_{j+1/2}$ is designed to be zero in regions of smooth flow and near one in regions with discontinuities. It varies from one grid point to another and is obtained either from a wavelet analysis of the solution (WAV-filter scheme), or from a gradient-based detector (ACM-filter scheme) [27, 28, 18, 29, 21]. The blending of nonlinear filters with high order linear filter is discussed in [29].

The dissipative portion of the nonlinear filter $\phi^l_{j+1/2} = g^l_{j+1/2} - b^l_{j+1/2}$ is the dissipative portion of a high order high-resolution shock-capturing scheme for the lth-characteristic wave. Here $g^l_{j+1/2}$ and $b^l_{j+1/2}$ are numerical fluxes of the uniformly high order high-resolution scheme and a high order central scheme for the lth characteristic, respectively. It is noted that $b^l_{j+1/2}$ might not be unique since there is more than one way of obtaining $\phi^l_{j+1/2}$. For the forms of the $\phi^l_{j+1/2}$ used in the numerical experiment section, see [27, 28, 18, 29, 21]. For example, the form of Harten and Yee and symmetric TVD schemes are already in the proper form in the sense that they are written in a central differencing portion $b^l_{j+1/2}$ and a nonlinear dissipation portion $\phi^l_{j+1/2}$. No work is required to obtain $\phi^l_{j+1/2}$ in this case.

With the exception of some smooth flows using the WAV-filter scheme, the filter given by (6), if applied to the entire MHD system (denoted by "filter all") normally will not preserve the divergence free magnetic field condition. In order to minimize the numerical error of the divergence-free magnetic condition, the nonlinear filter step only acts on the gas dynamic portion of the equations (denoted by "no filter on $\mathbf{B}$"). With the divergence free spatial base scheme and the manner that we update the solution on the filter step, the divergence free property should be preserved by the "no filter on $\mathbf{B}$" option. There are additional variants of the filter approach that from a theoretical standpoint, are divergence free. See [30] for more details.

4 2-D Compressible MHD Numerical Examples

For illustrative purposes, numerical experiments using sixth-order central spatial discretization as the base scheme is chosen for the ACM-filter and WAV-filter schemes. The sixth-order base scheme together with the nonlinear/linear filter with wavelet sensor will be denoted WAV66. When a more conventional gradient based sensor ACM is used, the scheme is denoted ACM66. If high order linear numerical dissipation is also used in the base scheme, the methods will be denoted WAV66+AD8 and ACM66+AD8 respectively. The strength of the eighth-order dissipation will be denoted by a tunable coefficient d, as in (4). In all of the filter scheme computations, the nonlinear dissipative portion of Harten-Yee is used as part of the nonlinear filter term. For all test cases, the entropy fix parameter is 0.25 for the ACM and WAV-filter schemes.

The fifth-order weighted ENO scheme [12] (WENO5), and second-order Harten-Yee and MUSCL schemes are used for comparison. Classical fourth-order Runge-Kutta time stepping is used for all sixth-order schemes, as well as for the WENO5 scheme. The second-order Harten-Yee and MUSCL are integrated in time by the second-order TVD Runge-Kutta method. Except for WENO5, the minmod limiter, the van Leer version of the van Albada limiter and the Colella-Woodward limiter are considered.

The $\nabla\cdot\mathbf{B}$ numerical error is obtained by approximating the spatial derivatives by sixth-order centered differences for WAV66, ACM66 and WENO5, whereas the corresponding $\nabla\cdot\mathbf{B}$ numerical error is obtained by second-order centered differences for the second-order TVD schemes (MUSCL and Harten-Yee). The L^2-norm of $\nabla\cdot\mathbf{B}$ of a particular scheme is computed by taking the square root of the sum over the square of all three spatial directions of the discretized form of $\nabla\cdot\mathbf{B}$ at all grid points.

4.1 MHD Kelvin-Helmholtz Instabilities ($\gamma = 1.4$, Periodic BC)

The magnetohydrodynamic Kelvin-Helmholtz instabilities have been studied by many previous investigators [2, 13, 8]. We have used the set up in [2] which is shown in Fig. 1. Snapshots of the time evolution of the x-velocity is also shown in Fig. 1 by CEN66+AD8 (sixth-order central with an eighth-order linear dissipative added to the base scheme ($d = 0.001$). The solution is obtained without the filter step. At stopping time $T = 0.5$, the problem is smooth enough that it can be solved by the base scheme alone. Density contours at time $T = 0.5$ with 30 equidistant contour levels between 0.4 and 1.2 are used. Five levels of grid refinement are considered, namely, 51×101, 101×201, 201×401, 401×801 and 801×1601. Grids of increasing refinements by the eighth-order central difference with a tenth-order linear dissipation added (CEN88+AD10, $d = 0.001$) are used as the reference solution. Computations using $d = 0$ (CEN88) are not stable for the five grids.

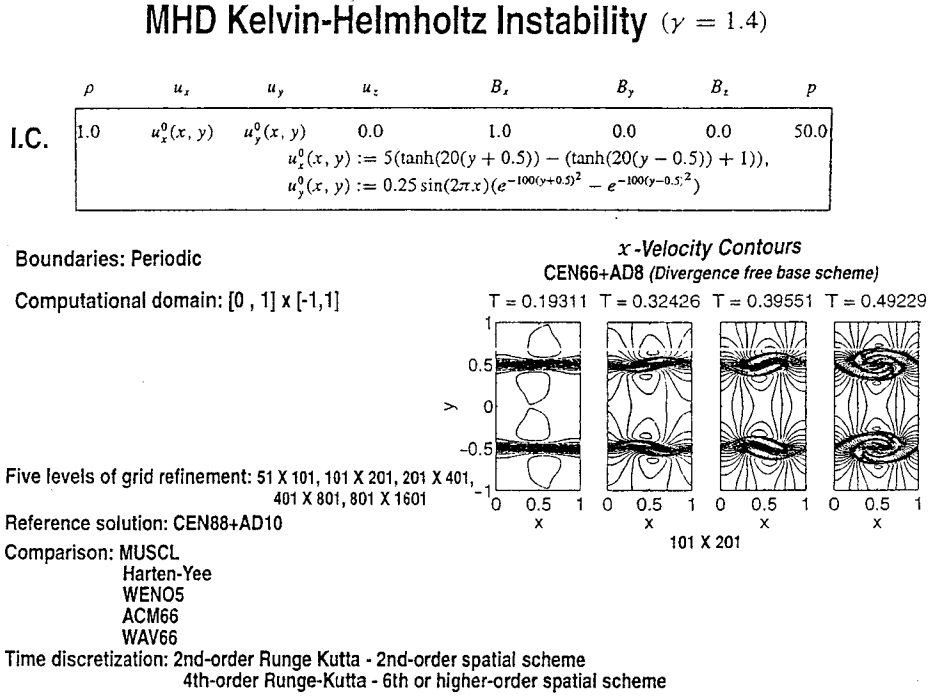

Fig. 1. Problem setup and time evolution of the Kelvin-Helmholtz problem. x-velocity contours by CEN66+AD8 on 101×201 grid points.

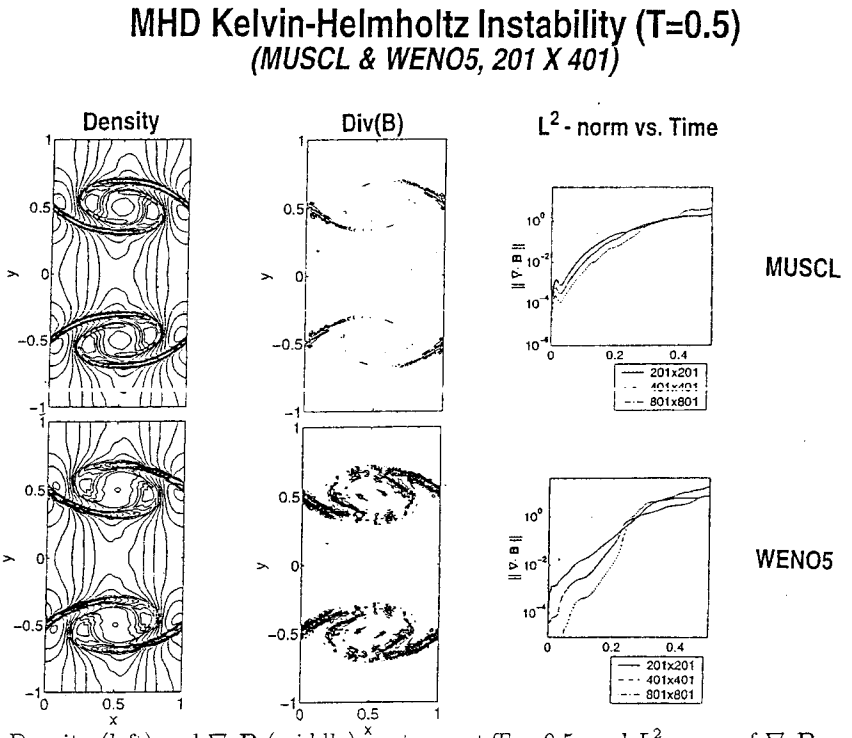

Fig. 2. Density (left) and $\nabla \cdot \mathbf{B}$ (middle) contours at $T = 0.5$, and L^2-norm of $\nabla \cdot \mathbf{B}$ as a function of time (right) by MUSCL (top row) and WENO5 (bottom row).

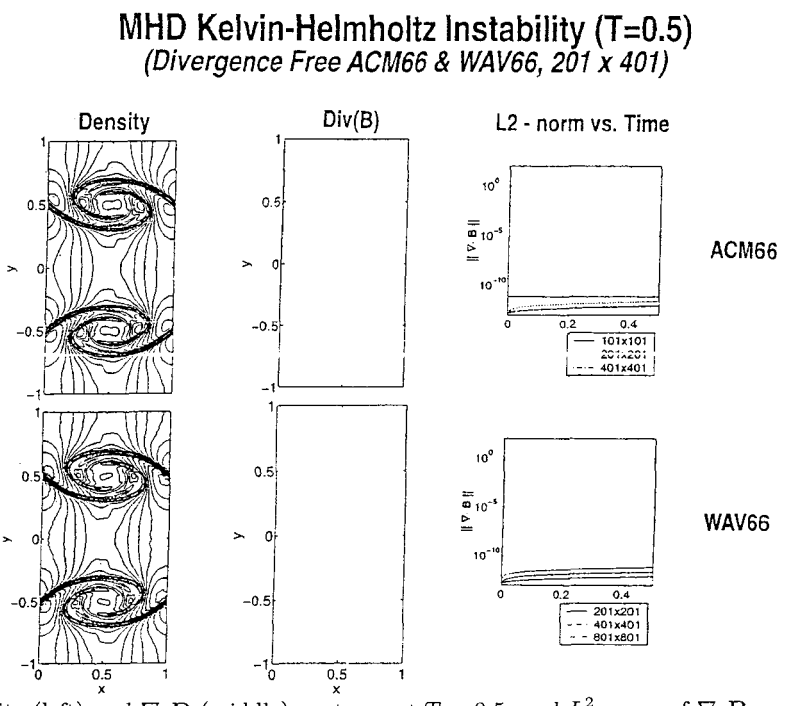

Fig. 3. Density (left) and $\nabla\cdot\mathbf{B}$ (middle) contours at $T = 0.5$, and L^2-norm of $\nabla\cdot\mathbf{B}$ as a function of time (right) by ACM66 (top row) and WAV66 (bottom row).

At time 0.5 the problem is smooth enough and there is no need for the more CPU intensive shock-capturing schemes. However, as the flow evolves at a later time, shock-capturing methods are required. Here, the purpose is to examine the $\nabla\cdot\mathbf{B}$ numerical error when the flow is still smooth using shock-capturing methods. Figure 2 shows the density (left) and $\nabla\cdot\mathbf{B}$ (middle) contours at $T = 0.5$, and L^2-norm of $\nabla\cdot\mathbf{B}$ as a function of time (right) by MUSCL (top row) and WENO5 (bottom row). The same computations by ACM66 and WAV66 are shown in Fig. 3. The $\nabla\cdot\mathbf{B}$ contours with 30 equidistant contour levels between -150 and 150 are used. The CPU time used was considerably larger (around a factor 2.5) for the WENO5 scheme. MUSCL, Harten-Yee and WENO5 exhibit small oscillations at the outer edges of the vortices as the grid is refined. It is possible to decrease these oscillations by increasing the multi-dimensional entropy fix parameters of the Harten-Yee scheme [26].

Density contours using ACM66, ACM66+AD8, WAV66 and WAV66+AD8 for all limiters exhibit an accuracy similar to CEN88+AD8 (figures not shown). There is no gain in solving the conservative over the non-conservative system for these two filter schemes. However, their $\nabla\cdot\mathbf{B}$ numerical errors are very different when using the "no filter on $\mathbf{B}$" option verses the "filter all" option. They are also very different from the standard MUSCL, Harten-Yee and WENO5 schemes. For the no filter on B equations option, divergence free preservation is achieved by the ACM66 and WAV66. The three standard shock-capturing methods exhibit similar $\nabla\cdot\mathbf{B}$ numerical errors.

4.2 A 2-D Compressible MHD Riemann Problem ($\gamma = 5/3$, Dirichlet BC)

We examine the same 2-D Riemann problem as in [2]. It consists of four constant states at time zero, as shown in Fig. 4. Grid convergence studies solving conservative (top) and

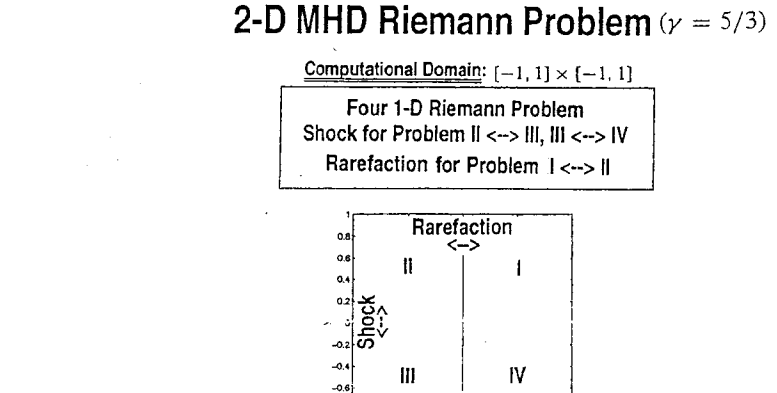

I.C.

Qdr.	ρ	ρu_x	ρu_y	ρu_z	B_x	B_y	B_z	e
I	0.9308	1.4557	−0.4633	0.0575	0.3501	0.9830	0.3050	5.0838
II	1.0304	1.5774	−1.0455	−0.1016	0.3501	0.5078	0.1576	5.7813
III	1.0000	1.7500	−1.0000	0.0000	0.5642	0.5078	0.2539	6.0000
IV	1.8887	0.2334	−1.7422	0.0733	0.5642	0.9830	0.4915	12.999

Fig. 4. Schematic of the initial data for the 2-D Riemann problem.

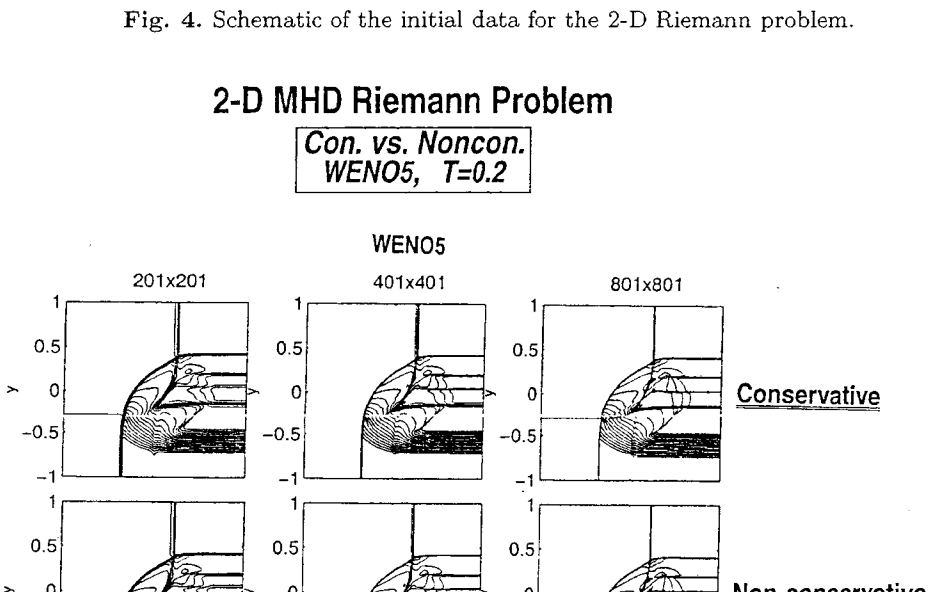

Fig. 5. Grid refinement by WENO5. Density contours solving the conservative (upper row) and non-conservative (lower row) form of the equations.

non-conservative (bottom) system by WENO5 are shown in Fig. 5 for density contours at $T = 0.2$ with 40 contours equally spaced between 0.75 and 2.1.

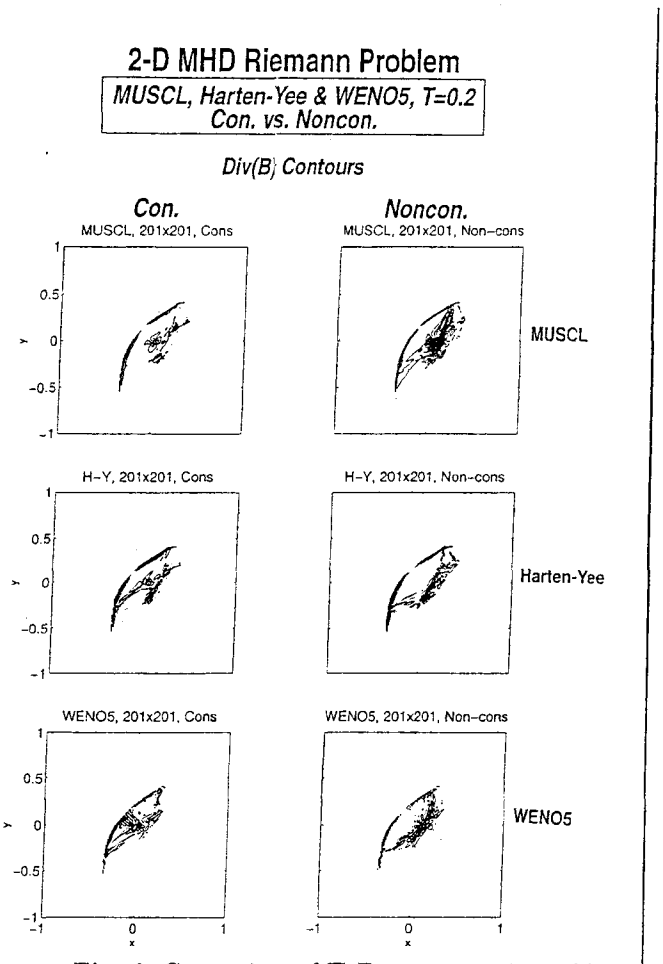

Fig. 6. Comparison of $\nabla \cdot \mathbf{B}$ contours using a 201×201 grid.

The accuracy in a solution of a Riemann problem away from discontinuities is difficult to improve by increasing the order of the scheme. A large part of the solution is constant, and the structure that develops is affected by low order errors from the discontinuity in the initial data. Since all five methods can capture shocks within 2-4 grid cells, their density contours look very similar even-though the $\nabla \cdot \mathbf{B}$ contours or the L_2 norm of the $\nabla \cdot \mathbf{B}$ numerical errors are all very different.

The effect on $\nabla \cdot \mathbf{B}$ when switching from a non-conservative system to a conservative system is less significant for the Harten-Yee and WENO5 than for MUSCL. $\nabla \cdot \mathbf{B}$ contours for the three methods, MUSCL, Harten-Yee, and WENO5 are displayed in Fig. 6. The $\nabla \cdot \mathbf{B}$ contours use 30 equidistant contour levels between -3.7 and 3.7. The ACM66, ACM66+AD8 WAV66 and WAV66+AD8 methods all exhibit divergence free preservation when no nonlinear filter is applied on the $\mathbf{B}$ equations. Figures 7 show a comparison.

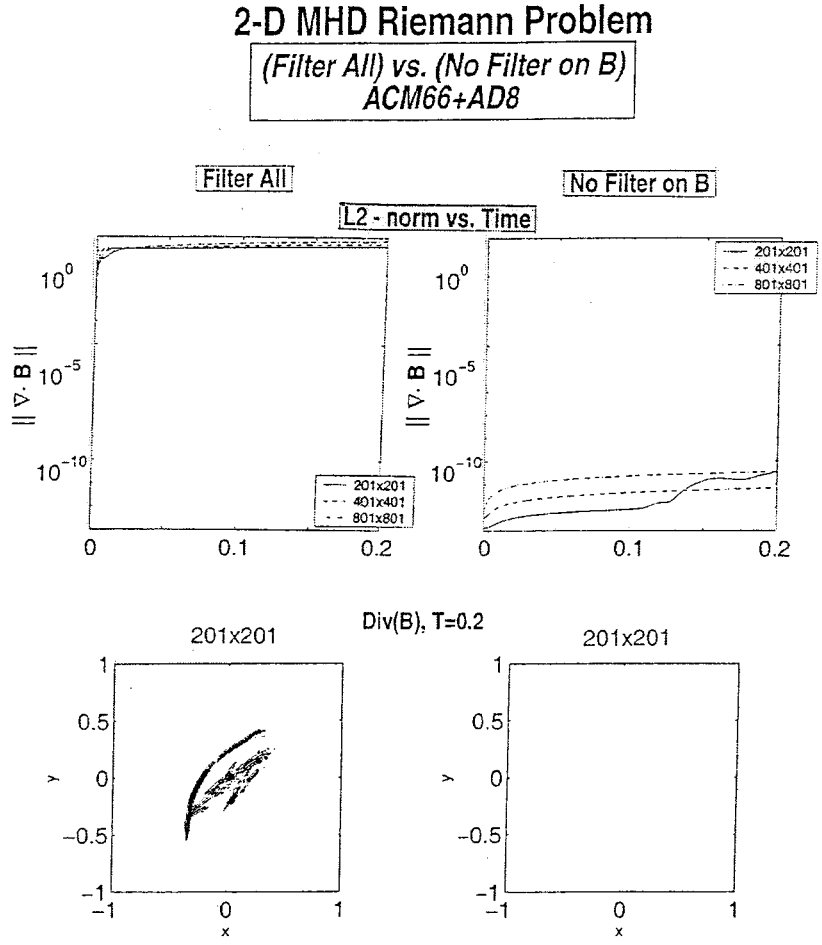

Fig. 7. L^2 norm of $\nabla \cdot \mathbf{B}$ vs. time and $\nabla \cdot \mathbf{B}$ contours at $T = 0.2$ by ACM66+AD8 when the nonlinear filter is not applied on the magnetic field (left) and when it is applied to all components (right). 201×201, 401×401, and 801×801 grid points.

4.3 Compressible MHD Orszag-Tang Vortex ($\gamma = 5/3$, Periodic BC)

The 2-D Compressible MHD Orszag-Tang vortex problem [14, 3, 15, 4, 5] consists of periodic boundary conditions with smooth initial data is shown in Fig. 8. Density contours by WAV66+AD8 at $T = 3.14$ using "filter all" and "no filter on $\mathbf{B}$" are shown in the same figure. The density contours are almost identical.

The initial sine waves break into discontinuities at a later time with complicated flow interactions. The computation stops at time T= 3.14 ($\approx \pi$), when discontinuities have formed and interacted. The solution has both complicated structure and discontinuities. It is a problem well suited for demonstrating our approach with highly accurate methods for solutions with discontinuities. Density contours with 30 equally spaced contours between 0.9 and 6.1 are used for illustration. Again, the same five levels of grid refinement study were performed on all five methods.

Figures 9 and 10 show the comparison of WENO5 (solving both systems) with WAV66+AD8. Divergence free preservation is achieved by WAV66+AD8 using the "no

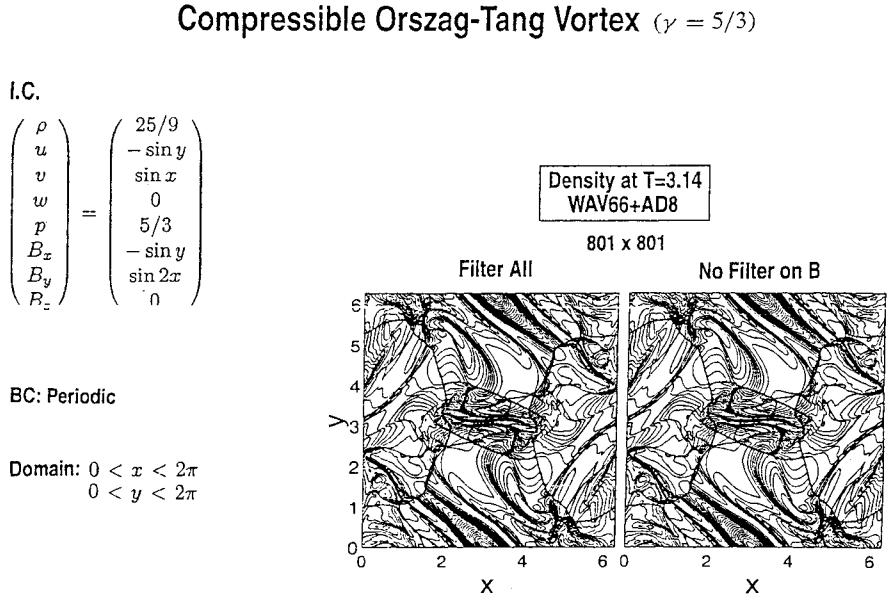

Fig. 8. Schematic, problem setup and density contours by WAV66+AD8 for the Orszag-Tang problem using a 801×801 grid at time $T = 3.14$.

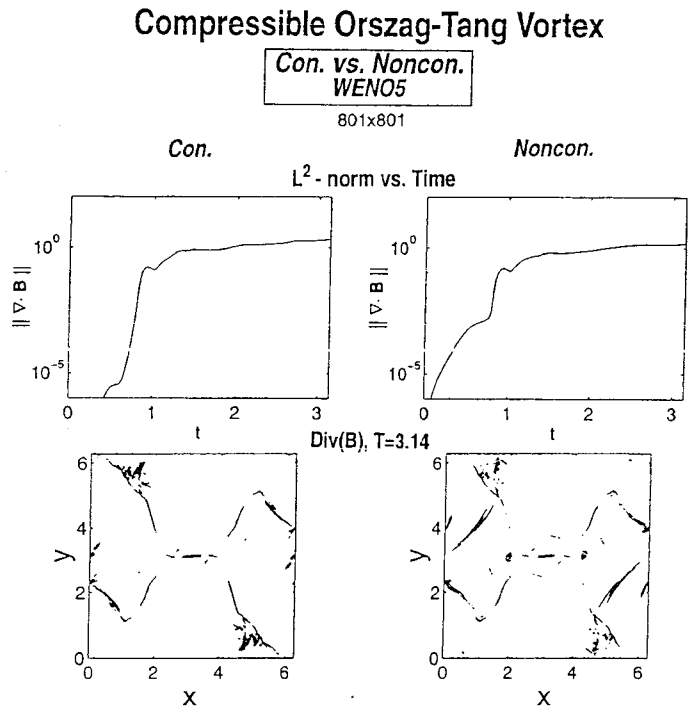

Fig. 9. L^2 norm of $\nabla \cdot \mathbf{B}$ in time (top) and $\nabla \cdot \mathbf{B}$ contours (bottom) by WENO5 for the conservative (left) and the non-conservative (right) systems.

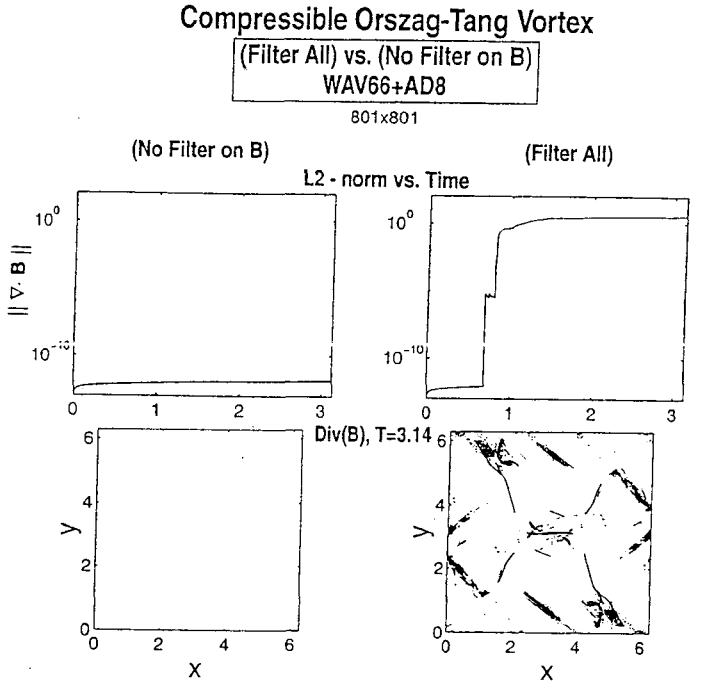

Fig. 10. WAV66+AD8 L^2 norm of $\nabla \cdot \mathbf{B}$ in time (top row), $\nabla \cdot \mathbf{B}$ contours at $T = 3.14$ (bottom row). No non-linear filter on $\mathbf{B}$ (left) and non-linear filter on all components (right).

filter on $\mathbf{B}$" option. ACM66+AD8 exhibits a similar behavior as WAV66+AD8 with the exception that divergence free is also possible for the "filter all" option for WAV66+AD8 for $T < 0.7$, whereas the ACM66+AD8 losses its divergence free preservation at a much earlier time. The behavior of WAV66 ($d = 0$) and ACM66 ($d = 0$) is similar.

The resolution of the global structure of the density contours is well captured by all five methods. However, small fine structures were captured by the ACM-filter and WAV-filter schemes on a 101×101 grid, and not by MUSCL, Harten-Yee and WENO5.

4.4 A Planar Shock Interacting with a Magnetic Cloud ($\gamma = 5/3$, Supersonic Inflow & Open Boundaries)

The fourth test problem is a planar shock interacting with a magnetic cloud studied in [4, 5]. This is a more challenging problem to simulate. The same initial configuration as in [23] is considered here. The problem setup and schematic of the initial condition is shown in Fig. 11. Figure 11 also shows the density contours by WENO5 at $T = 0.06$. Figures 12 and 13 show the same comparison between WENO5 and WAV66+AD8 as the previous problem. The behavior of ACM66+AD8, WAV66+AD8, WAV66 ($d = 0$) and ACM66 ($d = 0$) is similar to the Orszag-Tang problem. The same conclusion can be drawn for evolution time up to $T = 0.04$.

This problem is very stiff and very small CFL is required. For the finer grid, in order to obtain a stable solution by WENO5, the CPU time is more than an order of magnitude greater than for the Harten-Yee and MUSCL schemes, and many times more CPU than the ACM and WAV-filter scheme. This is partially due to a lower stability limit of WENO5 than the rest of the schemes. For all four test cases, MUSCL and Harten-Yee require similar CPU. The ACM and WAV-filter schemes require slightly more CPU than the Harten-Yee and MUSCL schemes. For almost all problems, WENO5 requires more CPU than ACM

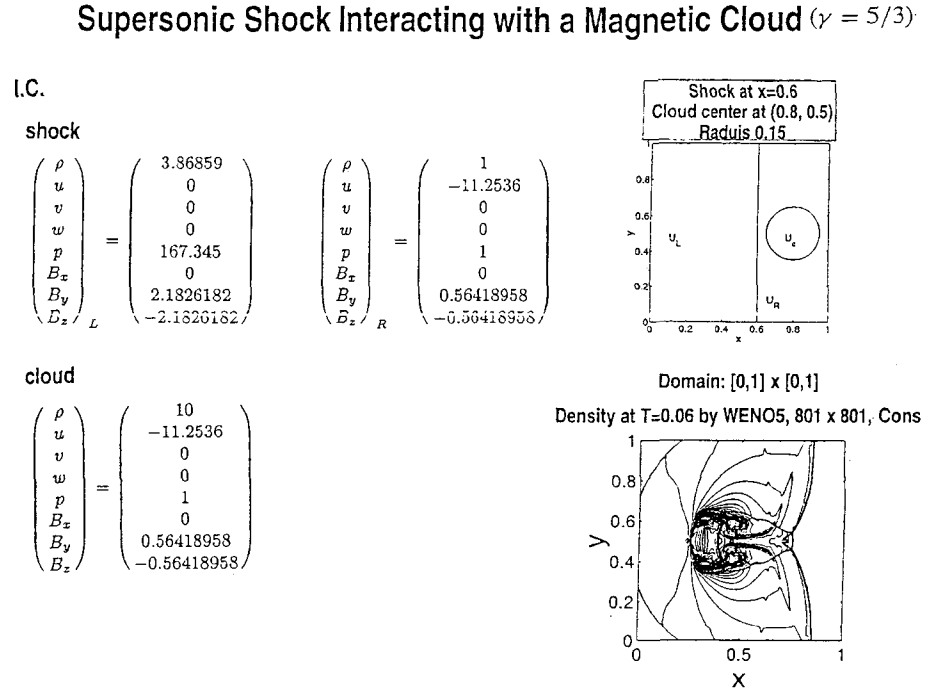

Fig. 11. Problem setup and schematic of the initial data of the MHD shock/cloud interaction problem. Density contours by WENO5 solving the conservative system using a 801 × 801 grid.

and WAV-filter schemes. In addition, for all test cases and all five methods, the $\nabla \cdot \mathbf{B}$ contour numerical errors (at their corresponding stopping times) increase as the grid is refined. For a detailed comparison and the performance of all five schemes of all the test cases, see [30].

5 Concluding Remarks

A natural and efficient high order filter approach in the sense of not needing traditional divergence cleaning for the minimization of the $\nabla \cdot \mathbf{B}$ numerical error was proposed and validated using four 2-D compressible MHD test cases. Five levels of grid refinement on four different flow types were compared with three standard high-resolution shock-capturing schemes, namely, a second-order MUSCL and Harten-Yee upwind TVD schemes, and the fifth-order WENO scheme. The role that the proper treatment of the corresponding numerical boundary conditions can play on the effect of reducing the $\nabla \cdot \mathbf{B}$ numerical error was studied in [30]. Among the four test cases, with the exception of the MHD shock/cloud interaction problem, we can safely conclude that divergence free high order filter schemes for the compressible MHD equations are possible without the need of standard divergence cleaning. These schemes are applicable to a wide variety of flow physics problems. Application of these schemes to viscous MHD flows with resistivity and multiscale structure is forthcoming.

References

1. P. Cargo and G. Gallice, *Roe Matrices for Ideal MHD and Systematic Construction of Roe*

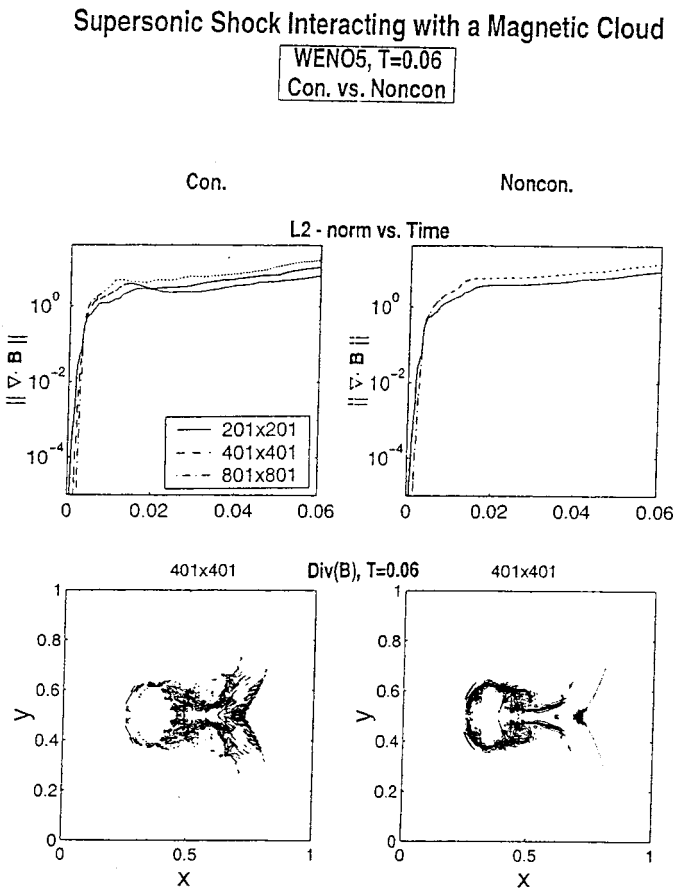

Fig. 12. Grid convergence study of L^2-norm of $\nabla \cdot \mathbf{B}$, and $\nabla \cdot \mathbf{B}$ contours at $T = 0.06$ by WENO5 using a 401×401 grid, conservative (left) and non-conservative (right).

Matrices for Systems of Conservation Laws, J. Comput. Phys., **136** (1997), pp. 446-466.

2. A. Dedner, F. Kemm, D. Kröner, C.-D. Munz, T. Schnitzer, and M. Wesenberg, *Hyperbolic Divergence Cleaning for the MHD Equations*, J. Comput. Phys., **175** (2002), pp. 645–673.
3. R.B. Dahlburg and J.M. Picone, *Evolution of the Orszag-Tang Vortex System in a Compressible Medium. I. Initial Average Subsonic Flow,* Phys. fluid B, **1**, (1989), pp. 2153-???.
4. W. Dai and P. R. Woodward, *A Simple Finite Difference Scheme for Multidimensional Magnetohydrodynamical Equations* J. Comput. Phys., **142** (1998), pp. 331-369.
5. W. Dai and P.R. Woodward, *On the Divergence-Free Condition and Conservation Laws in Numerical Simulations for Supersonic Magnetohydrodynamic Flows,* Astrophys. J., **494**, (1998), pp. 317-335.
6. H. De Sterck, *Multi-Dimensional Upwind Constrained Transport on Unstructured Grids for Shallow Water Magnetohydrodynamics*, AIAA Paper 2001-2623, (2001).
7. C.R. Evans and J.F. Hawley, *Simulation of Magnetohydrodynamic Flows: A Constrained Transport Method*, Astrophys. J. **332**, (1988), pp. 659–677.
8. A. Frank, T.W. Jone, D. Ryu and J.B. Gaalaas, *The Magnetohydrodynamic Kelvin-Helmholtz Instability: A Two- Dimensional Study,* Astrophys. J. **460**, (1996), pp. 777-???.
9. G. Gallice, *Systéme dÉuler-Poisson, Magnétohydrodynamique et Schemeas de Roe*, PhD Thesis, L'Université Bordeaux I, 1997.
10. S.K. Godunov *An Interesting Class of Quasilinear Systems,* Dokl. Akad, Nauk SSSR, **139**, (1972), pp. 521-523.
11. A. Harten and J.M. Hyman, *A Self-Adjusting Grid for the Computation of Weak Solutions of Hyperbolic Conservation Laws,*, J. Comput. Phys., **50**, (1983), pp. 235–269,

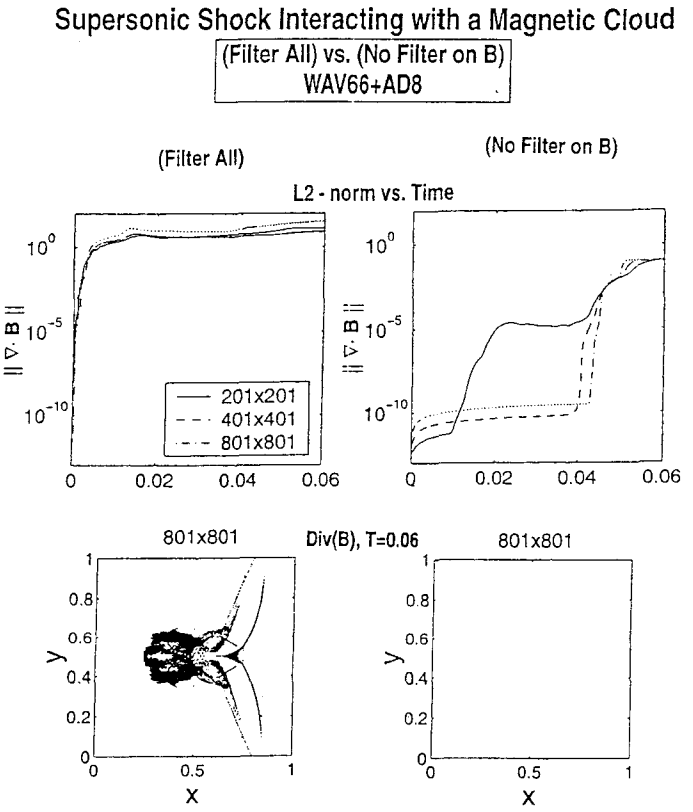

Fig. 13. Grid convergence study of L^2-norm of $\nabla \cdot \mathbf{B}$, and $\nabla \cdot \mathbf{B}$ contours at $T = 0.06$ by WAV66+AD8 using a 801×801 grid, filter all (left) and no filter on $\mathbf{B}$ (right).

12. G.-S. Jiang and C.-W. Shu, *Efficient Implementation of Weighted ENO schemes*, J. Comput. Phys., **126** (1996), pp. 202–228.
13. A. Malagoli, G. Bodo and R. Rosner, *On the Nonlinear Evolution of Magnetohydrodynamic Kelvin-Helmholtz Instabilities'* Astrophys. J. **456**, (1996), pp. 708-???.
14. S.A. Orszag and C.M. Tang *Small Scale Structure of Two-Dimensional Magnetohydrodynamic* Turbulence, J. Fluid Mech., **90**, (1979), pp. 129-???.
15. J.M. Picone and R.B. Dahlburg, *Evolution of the Orszag-Tang Vortex System in a Compressible Medium. II. Supersonic Flow,* Phys. Fluid B, **3**, (1991), pp. 29-???.
16. K.G. Powell, *An Approximate Riemann Solver for Magnetohydrodynamics (That works in More than One Dimension),* ICASE-Report 94-24, NASA Langley Research Center, April 1994.
17. K.G. Powell, P.L. Roe, T.J. Linde, T.I. Gombosi and D.L. De Zeeuw, *A Solution-Adaptive Upwind Scheme for Ideal Magnetohydrodynamics*, J. Comput. Phys., **154** (1999), pp. 284-309.
18. B. Sjögreen and H. C. Yee, *Multiresolution Wavelet Based Adaptive Numerical Dissipation Control for Shock-Turbulence Computation*, RIACS Technical Report TR01.01, NASA Ames research center (Oct 2000), to appear, J. Scient. Computing.
19. B. Sjögreen and H. C. Yee, *Grid Convergence of High Order Methods for Multiscale Complex Unsteady Viscous Compressible Flows*, RIACS Technical Report TR01.06, April, 2001, NASA Ames research center; AIAA 2001-2599, Proceedings of the 15th AIAA CFD Conference, June 11-14, 2001, Anaheim, CA., also, J. Comput. Phys., **185**, (2003), pp. 1-26.
20. B. Sjögreen and H. C. Yee, *Low Dissipative High Order Numerical Simulations of Supersonic Reactive Flows*, RIACS Technical Report TR01-017, NASA Ames Research Center (May 2001); Proceedings of the ECCOMAS Computational Fluid Dynamics Conference 2001, Swansea, Wales, UK, September 4-7, 2001.

21. B. Sjögreen and H. C. Yee, *Analysis of High Order Difference Methods for Multiscale Complex Compressible Flows*, Proceedings of the 9th International Conference on Hyperbolic Problems, March 25-29, 2002, Pasadena, CA.
22. B. Sjögreen and H.C. Yee, *Efficient Low Dissipative High Order Schemes for Multiscale MHD Flows, I: Basic Theory*, AIAA 2003-4118, Proceedings of the 16th AIAA/CFD Conference, June 23-26, 2003, Orlando, Fl.
23. G. Tóth, *The div B=0 Constraint in Shock-Capturing Magnetohydrodynamic Codes*, J. Comput. Phys., **161**, (2000), pp. 605-652.
24. M. Vinokur, *A rigorous derivation of the MHD Equations Based only on Faraday's and Ampére's Laws,* Presentation at LANL MHD Workshop on $\nabla \cdot \mathbf{B}$ Cleaning, August, 1996.
25. M. Vinokur and H.C. Yee, *Extension of Efficient Low Dissipative High Order Schemes for 3-D Curvilinear Moving Grids,* NASA TM 209598, June 2000.
26. H.C. Yee, *A Class of High-Resolution Explicit and Implicit Shock-Capturing Methods*, VKI Lecture Series 1989-04, March 6-10, 1989, also NASA TM-101088, Feb. 1989.
27. H.C. Yee, N.D. Sandham, N.D., and M.J. Djomehri, *Low Dissipative High Order Shock-Capturing Methods Using Characteristic-Based Filters*, J. Comput. Phys., **150** (1999) pp. 199-238.
28. H.C. Yee, M. Vinokur, M., and M.J. Djomehri, *Entropy Splitting and Numerical Dissipation*, J. Comput. Phys., **162** (2000) pp. 33-81.
29. H.C. Yee and B. Sjögreen, *Designing Adaptive Low Dissipative High Order Schemes for Long-Time Integrations*, **Turbulent Flow Computation**, (Eds. D. Drikakis & B. Geurts), Kluwer Academic Publisher (2002); also RIACS Technical Report TR01-28, Dec. 2001.
30. H.C. Yee and B. Sjögreen, *Efficient Low Dissipative High Order Schemes for Multiscale MHD Flows, II: Minimization of* $\nabla \cdot \mathbf{B}$ *Numerical Error* RIACS Report, July 2003.
31. K.S.Yee, *Numerical solution of initial boundary value problems involving Maxwell's equations in isotropic media*, IEEE Trans. Antennas Propagat., **14** (1966), pp. 302–307.
32. A.L. Zachary, A. Malagoli and P. Colella, *A Higher-Order Godunov Method for Multidimensional Ideal Magnetohydrodynamics*, SIAM J. Sci. Comput., **15**, (1994), pp. 263-284.